الجمهورية الجزائرية الديمقراطية الشعبية
People's Democratic Republic of Algeria
وزارة التعليم العالي و البحث العلمي
Ministry of Higher Education and Scientific Research

المدرسة الوطنية العليا للتكنولوجيا و الهندسة - عنابة
National Higher School of Technology and Engineering – Annaba

Department of Process Engineering and Energetics

In Partial Fulfillment of the Requirements

for the Degree of

STATE ENGINEER

Field of Study: Chemical Engineering

Presented by

Mohamed Amine HAMDANE
Mohamed Rostoum BRAHIMI

Optimization of the electrocatalytic reduction of CO_2 to CH_3OH and CH_4 using experimental designs and HYSYS to simulate the process

Supervised by

Dr. Salima BENDEBANE
NHSTE Annaba

Examination Board :

- Dr. KAHALERAS Mohamed Said — President – ENSTI-Annaba
- Dr. CHAOUCHI Sarrah — Examiner – ENSTI-Annaba
- Dr. KERBOUA Kaouther — Examiner – ENSTI-Annaba
- Mr. HAMADI Karim — Guest – FERTIAL -Annaba

Academic Year 2025

Abstract

This study explores the conversion of carbon dioxide (CO_2) into valuable hydrocarbons, specifically methanol and methane, through electrocatalytic and electrochemical processes. In the first part, CO_2 was converted into methanol using a series of synthesized catalysts based on transition metals (Ni, Co, Cr) supported on TiO_2. A mixture design approach identified Co-Cr/TiO_2 as the most efficient catalyst. Under optimal conditions (0.045 g catalyst, 8 h reaction time, 4 A/dm² current density), a methanol concentration of 0,9048M was achieved. Catalyst stability tests revealed a maximum concentration of 1.5 M after 13 h, with gradual deactivation observed beyond this point.

The second part focused on optimizing the electrochemical conversion of CO_2 into methane using the previously produced methanol as a reaction medium. A full factorial design (2^2) showed that the best yield (327 mL of CH_4) was obtained at 0 °C and 3 V.

To assess industrial scalability, a process simulation was carried out using Aspen HYSYS V11, integrating methanol and methane production pathways. The results confirm the feasibility of converting CO_2 into energy-rich compounds under mild conditions, offering a sustainable solution for greenhouse gas mitigation.

Keywords

CO_2 valorization; Methanol production; Methane generation; Electrocatalysis; Catalyst stability; Response Surface Methodology (RSM); Aspen HYSYS simulation.

Résumé

Cette étude explore la conversion du dioxyde de carbone (CO_2) en hydrocarbures à forte valeur ajoutée, en particulier le méthanol et le méthane, par des procédés électrocatalytiques et électrochimiques. Dans la première partie, le CO_2 a été converti en méthanol à l'aide d'une série de catalyseurs synthétisés à base de métaux de transition (Ni, Co, Cr) supportés sur du TiO_2. Une approche par plan de mélange a permis d'identifier le catalyseur Co-Cr/TiO_2 comme le plus performant. Dans des conditions optimales (0,045 g de catalyseur, 8 h de réaction, densité de courant de 4 A/dm²), une concentration en méthanol de 0,9048M a été atteinte. Les tests de stabilité ont montré une concentration maximale de 1,5 M après 13 h, suivi d'une désactivation progressive du catalyseur.

La deuxième partie a porté sur l'optimisation de la conversion électrochimique du CO_2 en méthane, en utilisant le méthanol préalablement produit comme milieu réactionnel. Un plan factoriel complet (2^2) a montré que le meilleur rendement (327 mL de CH_4) a été obtenu à 0 °C et 3 V.

Pour évaluer la possibilité de mise à l'échelle industrielle, une simulation de procédé a été réalisée à l'aide du logiciel Aspen HYSYS V11, intégrant les voies de production du méthanol et du méthane. Les résultats confirment la faisabilité de la conversion du CO_2 en composés énergétiques dans des conditions douces, offrant une solution durable pour l'atténuation des gaz à effet de serre.

Mots-clés : Valorisation du CO_2 ; Production de méthanol ; Génération de méthane ; Électrocatalyse ; Stabilité catalytique ; Méthodologie des surfaces de réponse (RSM) ; Simulation Aspen HYSYS.

الملخص

تتناول هذه الدراسة تحويل ثاني أكسيد الكربون (CO_2) إلى هيدروكربونات ذات قيمة عالية، وخاصة الميثانول والميثان، باستخدام العمليات التحفيزية الكهربائية والإلكتروكيميائية. في الجزء الأول، تم تحويل CO_2 إلى ميثانول باستخدام مجموعة من المحفزات المُحضّرة المعتمدة على معادن انتقالية(Ni ، Co، Cr)مدعومة على TiO_2. وقد تم تحديد محفز-Co Cr/TiO_2كالأكثر فعالية باستخدام نهج تصميم خليط. تحت ظروف مثالية) 0.045 جرام من المحفز، 8 ساعات زمن التفاعل، كثافة تيار $A/dm^2 4$ ، تم الوصول إلى تركيز ميثانول قدره 0,9048 مول/لتر. أظهرت اختبارات الثبات التحفيزي تزكيزا أقصى قدره 1.5 مول/لتر بعد 13 ساعة، مع انخفاض تدريجي في النشاط بعد هذا الزمن. الجزء الثاني ركّز على تحسين عملية التحويل الإلكتروكيميائي لغازCO_2 إلى ميثان باستخدام الميثانول المنتج سابقًا كوسط تفاعل. أظهر تصميم تجريبي عاملين (2^2) أن أفضل ناتج) 327 مل من (CH_4 تم الحصول عليه عند درجة حرارة 0 م° وجهد 3 فولت.

ولأغراض التوسعة الصناعية، تم إجراء محاكاة للعملية باستخدام برنامجAspen HYSYS V11 ، حيث تم دمج مسارات إنتاج الميثانول والميثان. تؤكد النتائج إمكانية تحويل CO_2 إلى مركبات غنية بالطاقة تحت ظروف معتدلة، مما يوفر حلاً مستدامًا للحد من انبعاثات الغازات الدفيئة.

الكلمات المفتاحية :تحويل ثاني أكسيد الكربون؛ إنتاج الميثانول؛ توليد الميثان؛ التحفيز الكهربائي؛ استقرار المحفز؛ منهجية سطح الاستجابة(RSM) ؛ محاكاة.Aspen HYSYS

Acknowledgements

This thesis marks the end of a journey, but also the culmination of several months of hard work, dedication, moments of doubt, and valuable discoveries. As such, we would like to thank all the people who have each contributed in their way to this adventure.

We would first like to sincerely thank ***Mme Bendebane Salima*** *for her kind guidance, Since the beginning of this project, you have been able to guide us with skill and kindness; your wise advice, your expertise and your availability have been key elements in the development of our work; thanks to you, we have been able to deepen our thinking, refine our problem and develop a rigorous and relevant analysis. We would also like to thank you for your teaching; It is with emotion that we express our deep gratitude and respect.*

We also thank all the teachers we met during our course.

In particular, ***Mme Chaouchi Sarah*** *for her invaluable help, her support and her generosity. We have been through such difficult times that more than once we thought we would never see the end of the tunnel. In each of these moments, you have been there to strengthen us and help us find solutions. Thank you for your support, your kindness, and thank you for everything. We will never forget you.*

Dedication

With great pride, I dedicate my graduation and the joy I have long awaited to those who have always been a source of support ...

To the one whom words cannot describe, to the one who has always been and still is my greatest supporter in achieving my dreams, my refuge and my right hand, the one with the invisible hand that removed obstacles from my path, and whose prayers always carried my name day and night—my beloved and my inspiration, may God keep you in my life for as long as I live,

My dearest mother…

To the honorable one whose name I carry with pride, to the light that illuminated my path, to the man who devoted his entire life to see me climb the ladders of success, may God keep you in my life for as long as I live,

My dearest father…

To those through whom God strengthened me, and who have been the best supporters ***« My sisters »***

To those who lovingly stood by me in my times of weakness, in recognition of their support and in acknowledgment of their worth my second family ***« My maternal aunt and her family »***

Mohamed Amine

List of abbreviations

Symbol	Signification
CO_2	Carbone dioxide
CCU	Carbon Capture and Utilization
CNG	Compressed Natural Gas
SEM-EDS	Scanning Electron Microscopy
FTIR	Fourier Transform Infrared Spectroscopy
HER	Hydrogen Evolution Reaction
DOE	Design of Experiments
DRI	Direct Reduced Iron
BBD	Box Behnken Design
RSM	Response Surface Methodology
2D	Two dimensional
3D	Three dimensional

List of figures

Liste of tables

Table of content

General Introduction

Over the past few decades, the world has experienced an industrial revolution, which has contributed significantly to a dramatic rise in atmospheric carbon dioxide (CO_2) emissions. These emissions are primarily from fossil fuels, natural gas, etc. Which leads to serious environmental problems. For example, global warming, climate change, and the intensification of the greenhouse effect.

To face these major problems scientists and researchers are trying various methods to preserve the world, among their strategies we mention Carbon Capture and Utilization (CCU), its aim is not only to reduce CO_2 but also to transforming it into useful products like: methanol (CH_3OH) widely used in the manufacture of antifreeze, solvents, paints, fuels, and pesticides, and methane (CH_4) is a major component of biogas and compressed natural gas (CNG), with applications ranging from energy generation to fertilizer and chemical production, and various aldehydes. In this study, we're interested in one of the methods of CCU, which is the electrochemical reduction of CO_2. The principle of this method is the use of an electric current that passes through a cell to transform the reactants into products. This electric current can be replaced by a sustainable current source, such as solar or wind energy. Unlike conventional thermal conversion methods, the electrochemical reduction operates efficiently under ambient temperature and pressure conditions, significantly reducing energy consumption and operational hazards. To ensure the reaction, a catalyst should be introduced to the species, such as chromium-doped titanium dioxide (Cr/TiO_2), nickel-doped titanium dioxide (Ni/TiO_2), and cobalt-doped titanium dioxide (Co/TiO_2), to enhance reaction rates and selectivity. And in order to understand their efficiency and behavior, these catalysts undergo extensive characterization using techniques like Scanning Electron Microscopy (SEM-EDS) and Fourier Transform Infrared Spectroscopy (FTIR). However, one major problem is that the side reactions that can occur in aqueous electrochemical systems, such as the Hydrogen Evolution Reaction (HER), can compete with the electrochemical reduction, reducing the overall selectivity and efficiency of the process. Despite all of these advantages, another problem can be faced which is the quantity of the methanol and methane produced it will be in small amount and highly depending on the catalyst composition, electrochemical cell design, and operating conditions such as applied voltage and temperature.

The main goal of this research is to optimize this method to improve both yield and selectivity for methanol and methane by applying several materials for the electrode composition and varying the current intensity, and experimenting different types of catalysts and some mixtures with changing in quantity added each time to find the best result.

The research adopts a systematic approach by incorporating statistical design of experiments (DOE), specifically the Box-Behnken and mixture design models, to identify the optimal operating conditions for maximum yield. In addition to our lab work, a simulation using software called Aspen HYSYS (used for modeling and simulating various chemical and petrochemical processes) is done to scale up the process into a larger scale and not just in a small cell. This helps in the analysis of energy utilization, heat integration, and mass balance in downsizing from lab scale to industrial scale. Although the electrochemical part is hard to model accurately in HYSYS, we can at least model the recycle streams, the separator equipment, and the flows to view a whole system where CO_2 is being converted and the products are recovered

Chapter 1: Global and National Context of CO_2 Emissions

1.1. Global and National Overview of CO_2 Emissions

Carbon dioxide (CO_2) emissions continue to pose a serious global environmental challenge. Despite growing awareness and intensified climate policies, global CO_2 emissions increased by 0.8% compared to the previous year (2024). The main contributors to these emissions are anthropogenic activities, particularly the combustion of fossil fuels and industrial processes such as cement and ammonia production.

The world's largest economies remain the top emitters. China alone contributes over one-quarter of global CO_2 emissions, followed by North America, primarily the United States, and then Europe.

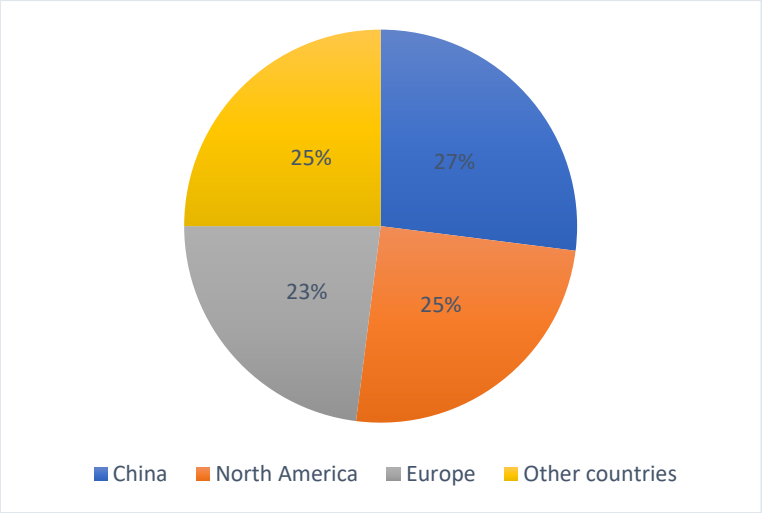

Figure 1.1. Major global CO_2 emitters.

In Algeria, fossil fuel-related CO_2 emissions were estimated at 180.4 million tonnes in 2023, representing a 3.37% decrease from the previous year. The average per capita emission was 3.99 tonnes, which is below the global average of 6.8 tonnes per capita recorded in 2022. The main contributors to Algeria's emissions are electricity and heat production, alongside the transportation sector. A significant portion of these emissions stems from natural gas combustion, underscoring the country's reliance on this energy source.

To address its carbon footprint, Algeria has committed to reducing its greenhouse gas emissions by 7% to 22% by 2030, as outlined in its Nationally Determined Contribution (NDC) under the Paris Agreement. These goals are to be achieved through an energy transition strategy and economic diversification efforts, including the installation of 15,000 MW of solar power by 2035. While these plans show strong intent, their successful implementation will be crucial in meeting national climate targets [1].

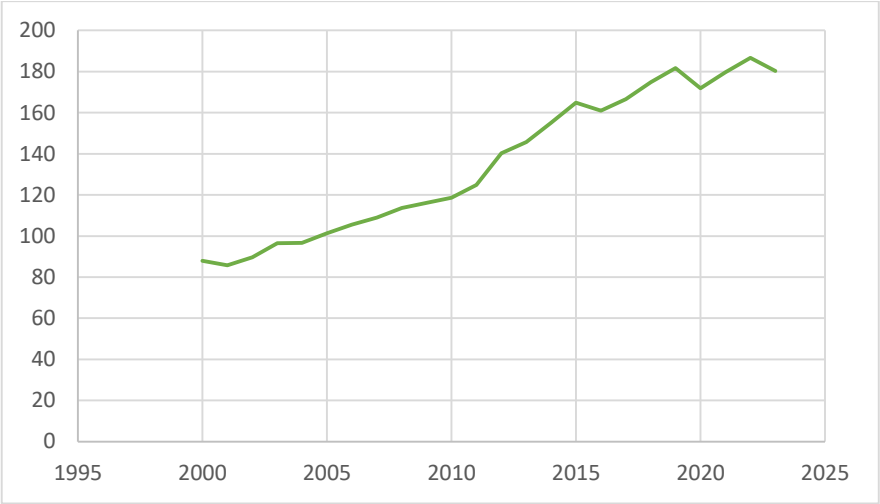

Figure 1.2. Evolution of CO_2 emissions in Algeria (2000–2023), in megatonnes.

1.2. CO_2 Emissions in Industry: The Case of Tosyali Oran

In Algeria, the industrial sector accounts for a significant share of CO_2 emissions, estimated at around 12% of total emissions five years ago. This includes approximately 5% from energy-related emissions and 7% from process-related emissions [2]. Between 1990 and 2019, industrial energy-related emissions increased by 32%, although the sector's emissions intensity decreased by 57% due to improved efficiency. Major emitting industries include iron and steel, cement, fossil fuels, and chemical manufacturing.

To align with a 1.5°C climate trajectory, carbon emissions from industrial energy use must decline by 73-79% by 2030, and reach near-zero levels by the early 2040s [2]. Key strategies to achieve this include increasing electrification from 25% in 2019 to 40-42% by 2030 and 77-83% by 2050, as well as integrating hydrogen and biomass into the industrial energy mix [2].

A prominent case study is Tosyali Algeria, located in Bethioua, Oran. As one of the world's leading direct reduced iron (DRI) producers, Tosyali operates a large-scale plant using the MIDREX® process. In this technology, iron ore is reduced using syngas (a mixture of CO and H_2) derived from natural gas. The main sources of CO_2 emissions in this process include:

1. The reformer unit, where natural gas is converted to CO and H_2, generating CO_2 as a by-product.
2. The reduction furnace, where iron ore (Fe_2O_3) is chemically reduced to metallic iron (Fe) by CO and H_2, releasing CO_2 and H_2O.
3. The electric arc furnace (EAF), used to melt DRI into steel, emits CO_2 depending on the electricity source.

Despite these emissions, Tosyali Algeria has made substantial progress in reducing its carbon footprint. In 2021, the plant set a world record by producing over 2.28 million tonnes of DRI, demonstrating high operational efficiency. Moreover, the company is currently investing in a second DRI plant with the capacity to use more hydrogen in place of natural gas, aligning with the global trend of using hydrogen as a cleaner reducing agent [3].

Through the adoption of advanced technologies and its commitment to sustainability, Tosyali Algeria contributes actively to Algeria's broader goals of industrial decarbonization and environmental responsibility [4].

Chapter 02: Literature Review

2.1. Introduction

For several decades, carbon dioxide (CO_2) has been explored as a valuable feedstock for the synthesis of fuels and chemical compounds. In recent years, increasing environmental concerns have further intensified research into its transformation through a variety of approaches, notably thermochemical, photochemical, photoelectrochemical, electrocatalytic, and hydrogenation-based methods. These techniques enable the conversion of CO_2 into more sustainable and reusable products, including methanol (CH_3OH), ethanol (C_2H_5OH), ethylene (C_2H_4), and methane (CH_4). The present study specifically targets the production of methanol and methane from CO_2, with a focus on hydrogenation and electrocatalysis, which have emerged as the most promising and efficient pathways for this purpose.

2.2. Hydrogenation of CO_2

Hydrogenation of carbon dioxide (CO_2) is one of the most extensively studied pathways for transforming carbon emissions into high-value energy carriers. This process involves the reaction of CO_2 with hydrogen (H_2), typically sourced from water electrolysis, in the presence of metallic catalysts. Among the main target products, methanol (CH_3OH) and methane (CH_4) stand out due to their widespread applications in energy, synthetic fuels, and green chemistry [5, 6]. Methanol synthesis is commonly catalyzed by $Cu/ZnO/ZrO_2$ systems operating under moderate temperatures (200-300 °C) and high pressures (around 50 bar). However, several critical challenges persist, including the need for green hydrogen to ensure a carbon-neutral footprint and the management of water formed during the reaction, which can deactivate active catalytic sites [7, 8].

On the other hand, CO_2 methanation via the Sabatier reaction ($CO_2 + 4H_2 \rightarrow CH_4 + 2H_2O$), typically catalyzed by nickel or ruthenium-based materials, offers a route to produce synthetic natural gas [9]. While thermodynamically favorable at low temperatures, this process demands catalysts with high resistance to thermal cycling and deactivation due to water accumulation or carbon deposition [10, 11]. Recent strategies have focused on the nanostructuring of catalysts and the engineering of supports to enhance selectivity and energy efficiency [12]. Although CO_2 hydrogenation is relatively mature, its industrial deployment remains heavily dependent on progress in sustainable catalyst design and the availability of low-carbon hydrogen.

2.3. Electrocatalysis of CO_2

Electrocatalytic reduction of carbon dioxide (CO_2) has attracted growing attention in recent years as a promising approach to transform CO_2 into valuable chemicals and fuels under mild conditions. Numerous studies have investigated how to improve the efficiency and selectivity of this process by exploring key parameters such as pressure, temperature, electrode material, pH, and electrolyte composition. One major challenge is the limited solubility of CO_2 in aqueous electrolytes. It has been observed that CO_2 solubility increases with pressure but decreases with temperature [13], thereby influencing the concentration of reactant available at the electrode surface [14]. The choice of electrode material is equally critical: copper (Cu), unlike most transition metals, uniquely facilitates the formation of hydrocarbons and alcohols such as methane (CH_4), ethylene (C_2H_4), and methanol (CH_3OH), making it a preferred electrocatalyst [15, 16].

Another fundamental factor influencing the CO_2 reduction reaction (CO_2RR) is the pH of the electrolyte. In alkaline solutions, CO_2 rapidly reacts with hydroxide ions (OH^-) to form bicarbonate (HCO_3^-) and carbonate (CO_3^{2-}), and in neutral environments CO_2 will also dissociate quickly into $HCOO^-$ ions, thereby reducing the concentration of free CO_2 available for electroreduction, [17]. For this reason, CO_2RR is generally performed in mildly acidic environments, where CO_2 remains in its molecular form and more readily participates in electrochemical reactions.However, such environments also favor the competing hydrogen evolution reaction (HER), which is thermodynamically more favorable than CO_2 reduction [18]. The coexistence of HER and CO_2RR at the cathode necessitates the design of highly selective catalysts that suppress hydrogen production while enhancing the formation of carbon-based products [19, 20]. Recent developments include the engineering of nanostructured Cu-based and bimetallic catalysts, as well as the integration of gas-diffusion electrodes (GDEs), which enhance CO_2 transport and reaction kinetics [21, 22]. Despite considerable progress, achieving high selectivity, conversion rates, and long-term stability under industrially relevant conditions remains a major challenge.

2.4. Catalysts

The electrocatalytic reduction of carbon dioxide (CO_2) to methanol represents a promising route for the sustainable production of high-value chemicals such as methanol (CH_3OH) and formic acid (HCOOH), depending on the catalyst employed. Due to the high thermodynamic stability and chemical inertness of the CO_2 molecule, its activation requires the use of highly efficient catalysts. Catalytic systems for CO_2 electroreduction can be broadly classified into homogeneous and heterogeneous phases. Homogeneous catalysts are typically based on transition metal complexes, such as tetraazamacrocyclic nickel or cobalt species, and although they operate at relatively low overpotentials (~0.2 V), they tend to exhibit modest Faradaic efficiencies, often limited to around 30% [23].

In contrast, heterogeneous catalysts, often in the form of thin films deposited onto conductive substrates, demonstrate enhanced stability and scalability. Metal-metal bonded polymeric catalysts, particularly those incorporating ruthenium or osmium, have shown exceptional performance in formic acid production, achieving Faradaic efficiencies of up to 90% under optimized conditions [24]. Recent studies have also explored molybdenum-based systems, such as molybdenum carbide (Mo_2C) nanoparticles supported on nitrogen-doped carbon nanotubes (N-CNTs), which have demonstrated Faradaic efficiencies of 80.4% for methanol synthesis at an applied potential of -1.1 V [25].

Furthermore, organic molecular catalysts such as pyridine and its derivatives have been shown to facilitate CO_2 reduction in homogeneous solution through stepwise hydrogenation mechanisms. These organo-hydride systems promote the conversion of CO_2 to methanol via intermediate species such as formic acid (HCOOH) and formaldehyde (HCHO). Despite operating at low overpotentials (~300 mV), they can achieve remarkably high Faradaic efficiencies, reaching up to 96% under controlled experimental conditions [26]. These developments highlight the crucial role of catalyst design and mechanistic understanding in enhancing the selectivity, energy efficiency, and scalability of CO_2 electroreduction pathways.

Chapter 03: Materials and Methods

3.1. Introduction

The fundamental principle of the electrochemical reduction of carbon dioxide (CO_2) in an aqueous medium involves simultaneous redox reactions occurring at the cathode and anode. Specifically, the formation of methanol (CH_3OH) at the cathode proceeds via a multi-electron transfer process, as described by the following half-cell reactions [19]:

- *At the cathode*: $CO_2 + 6H^+ + 6e^- \rightarrow CH_3OH + H_2O$

  Alternatively: $6H^+ + 6e^- \rightarrow 3H_2$ (hydrogen evolution reaction)
- *At the anode*: $3H_2O \rightarrow 1.5O_2 + 6H^+ + 6e^-$

By combining these half-reactions, the overall reaction can be written as:

$$CO_2 + 2H_2O \rightarrow CH_3OH + 1.5O_2$$

Two competing cathodic reactions consume electrons in this system: the desired CO_2 reduction to methanol and the undesired hydrogen evolution reaction (HER) resulting from water electrolysis. The selectivity of the process is thus highly dependent on catalyst design, reaction conditions (e.g., pH, overpotential), and electrode surface properties, which collectively determine whether electrons are preferentially used for CH_3OH formation or diverted toward hydrogen generation.

Additionally, the produced methanol will be exploited as an electrolyte for the production of methane following the following cathodic reaction:

$$CO_2 + 8H^+ + 8e^- \rightarrow CH_4 + 2H_2O$$

3.2. Experimantal Techniques

3.2.1. Product used

The following analytical-grade reagents were used in this study. Calcium carbonate ($CaCO_3$, ≥99%, Merck) and hydrochloric acid (HCl, ACS reagent, 37%, Sigma-Aldrich) were employed for CO_2 generation. Sulfuric acid (H_2SO_4, 95–98%, Sigma-Aldrich) was used to control the acidity of the reaction medium, while sodium sulfate (Na_2SO_4, ≥99%, Merck) served as the supporting electrolyte. For catalyst preparation, nickel(II) nitrate hexahydrate ($Ni(NO_3)_2 \cdot 6H_2O$, ≥98%, Sigma-Aldrich), cobalt(II) nitrate hexahydrate ($Co(NO_3)_2 \cdot 6H_2O$, ≥98%, Sigma-Aldrich), and chromium(III) nitrate nonahydrate ($Cr(NO_3)_3 \cdot 9H_2O$, ≥98%, Sigma-Aldrich) were used as metal precursors, and titanium dioxide (TiO_2, ≥99%, Sigma-Aldrich) as the support material.

3.2.2. Experimental Procedure

The experimental setup consisted of two interconnected sections (Figure 3.1): one for CO_2 generation and the other for its electrocatalytic conversion.

In the first step, CO_2 gas was generated in situ by reacting calcium carbonate ($CaCO_3$, 2,05 g) with hydrochloric acid (HCl, 2 M) inside a sealed glass vessel. The reaction proceeds as follows:

$$CaCO_3\ (s) + 2HCl\ (aq) \rightarrow CaCl_2\ (aq) + H_2O\ (l) + CO_2\ (g)$$

The released CO_2 was transferred via a plastic tube to a closed electrochemical reactor, which was continuously stirred using a magnetic stirrer to maintain homogeneity.

The electrochemical cell contained an aqueous electrolyte solution prepared with sulfuric acid (H_2SO_4, 0.01 M) to maintain a slightly acidic pH (~5-6), and sodium sulfate (Na_2SO_4, 0.05 M) as a supporting electrolyte to ensure stable ionic conductivity throughout the reaction.
Two copper electrodes were inserted into the electrolyte and connected to a direct current power supply. The electrodes were aligned in a parallel configuration, facing each other at a fixed distance to facilitate uniform current distribution and efficient charge transfer. The entire system was operated under ambient temperature and pressure conditions.
The reactor also included a selected heterogeneous catalyst (e.g., Ni/TiO_2, Cr/TiO_2, Co/TiO_2, or $Cr\text{-}Co/TiO_2$), which was suspended in the electrolyte. A controlled flow of CO_2 was continuously injected into the reactor at low to moderate rates to ensure sufficient saturation and effective contact with both the catalyst and electrodes.

Figure 3.1. The assembly used.

3.2.3. Preparation of catalysts

In this study, four catalysts were prepared: Ni/TiO_2, Cr/TiO_2, Co/TiO_2, and a mixed $Cr\text{-}Co/TiO_2$ catalyst. The preparation followed a wet impregnation method. First, the required amounts of metal precursors, nickel (II) nitrate hexahydrate, chromium (III) nitrate nonahydrate, and cobalt(II) nitrate hexahydrate, were accurately weighed and dissolved in distilled water under continuous magnetic stirring. To enhance the dispersion of metal ions and stabilize the solution, EDTA (ethylenediaminetetraacetic acid) was added as a chelating agent. Titanium dioxide (TiO_2) was then gradually incorporated into the solution, and the suspension was maintained under agitation at room temperature for 4 hours to promote the adsorption of metal ions onto the TiO_2 surface. The resulting mixture was gently heated to evaporate the solvent until a semi-solid paste formed. This paste was subsequently dried in an oven at 100 °C for 12 hours to remove residual moisture. Finally, the dried material was subjected to calcination at 500 °C for 4 hours to activate the metal oxides. After cooling to room temperature, the catalysts were stored in sealed containers for later use in electrochemical experiments.

3.2.4. Characterization techniques used

3.2.4.1. Refractive index

The quantification of methanol concentration in the reaction medium was performed using refractive index measurements. A calibration curve was first established using a series of standard solutions prepared from commercial methanol at known concentrations. The corresponding refractive indices were measured and plotted to obtain a reference curve (Figure 3.2). To ensure consistency and comparability of results, all refractive index values were corrected to a standard temperature of 20 °C using the following empirical formula:

$$\eta^{20} = \eta^{T} + 0.00045 \times (T - 20)$$

Where: η^{T} is the refractive index measured at temperature T, and η^{20} is the corrected value at 20 °C.

This correction accounts for the temperature-dependent variation in refractive index and allows for accurate estimation of methanol concentration from experimental samples.

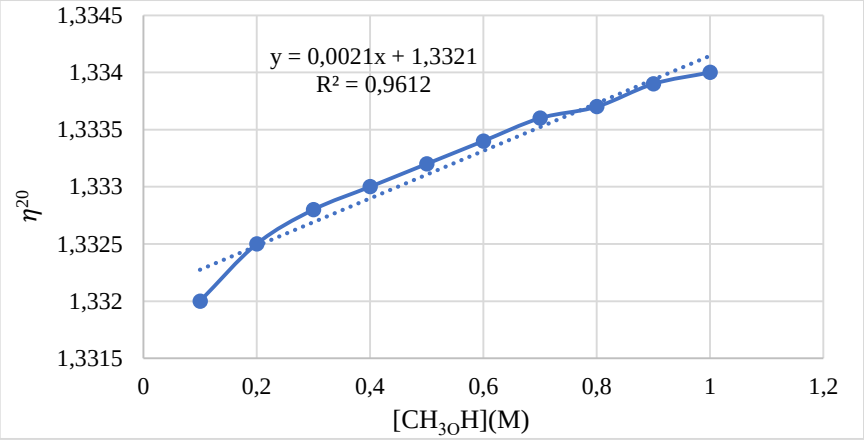

Figure3.2. Calibration curve

3.2.4.2. Characterization of Catalyst

- **SEM-EDS**

The morphology of the catalysts was examined using Scanning Electron Microscopy (SEM) with a Quanta FEI Quanta 250 instrument, operated via ZEISS control software. The microscope was equipped with an Energy Dispersive X-ray Spectroscopy (EDS) system, which facilitated the analysis of elemental composition, either as an average over the catalyst surface or at specific localized points.

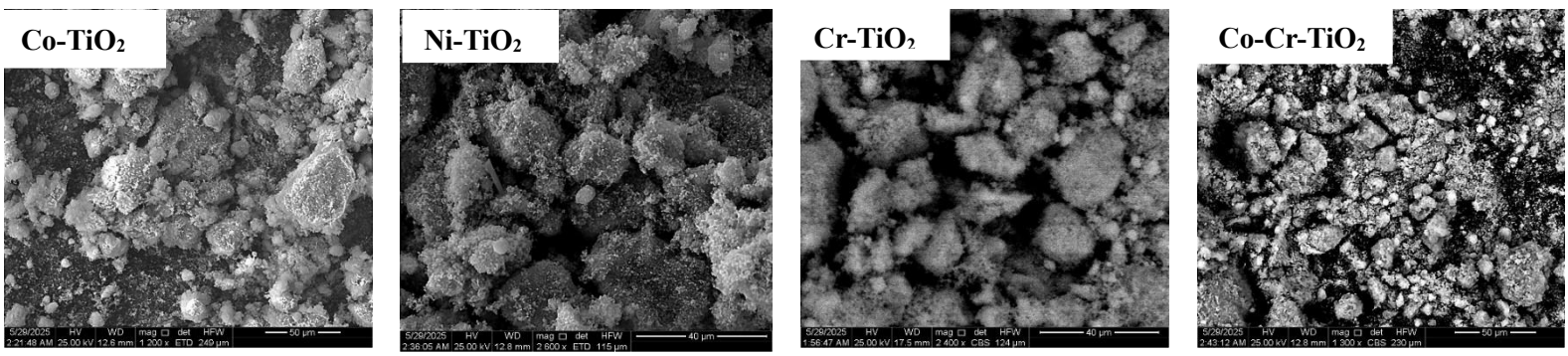

Figure 3.3. SEM of the catalysts used, taken at 30 µm

The SEM micrographs reveal clear morphological differences among the Co, Ni, Cr, and Co-Cr-based catalyst samples. The Co-doped sample exhibits large, irregular agglomerates with a rough surface, indicating high porosity but also a tendency toward particle aggregation, which could hinder access to active sites. Its average particle size, as shown in Table 3.3, is 8.85 μm, making it the coarsest among the four. The Ni-based catalyst shows the smallest average particle size (3.13 μm) and presents a granular, rough surface structure with fine particles dispersed across the matrix, suggesting high surface area and improved catalytic potential. The Cr-doped sample exhibits well-defined spherical particles with smoother surfaces and an average particle size of 5.06 μm, indicating good thermal stability but slightly reduced porosity. Lastly, the Co-Cr composite catalyst shows a more homogeneous distribution with moderately rough surfaces and an average particle size of 4.99 μm, reflecting a balance between dispersion and agglomeration. These morphological differences suggest that Ni and Co-Cr catalysts may offer better surface accessibility and active site exposure, making them promising candidates for catalytic applications such as CO_2 conversion or methanol synthesis.

Table 3.1. The average particle size of different catalysts used

Catalysts	**Co-TiO_2**	**Ni-TiO_2**	**Cr-TiO_2**	**Co-Cr-TiO_2**
Particle size (μm)	8.85	3.13	5.06	4.99

The elemental composition of the prepared catalysts, obtained by energy-dispersive X-ray spectroscopy (EDS), is summarized in Table 3.2. All samples show a dominant presence of titanium and oxygen, confirming the TiO_2 support as the main matrix. In the Co-TiO_2 sample, 0.05 wt.% of cobalt is successfully detected, while the Ni-TiO_2 sample contains 0.01 wt.% of nickel, indicating effective but minimal incorporation of the dopants. The Cr-TiO_2 catalyst shows 0.14 wt.% of chromium, associated with a noticeable decrease in Ti content due to partial substitution or surface deposition. In the Co-Cr-TiO_2 bimetallic system, both cobalt and chromium are present at 0.10 wt.% and 0.20 wt.%**,** respectively, suggesting successful co-doping. The observed variations in Ti and O content across the samples reflect the influence of metal loading and surface interaction with the TiO_2 support. These results confirm the effective integration of transition metals into the TiO_2 matrix, which can play a key role in tuning the catalytic properties.

Table 3.2. The average weight composition of the catalyst

	Co-TiO_2	**Ni-TiO_2**	**Cr-TiO_2**	**Co-Cr-TiO_2**
Ti (wt.%)	40.31	40.48	32.38	39.51
O (wt.%)	59.64	59.51	67.47	60.19
Ni (wt.%)	/	0.01	/	/
Co (wt.%)	0.05	/	/	0.10
Cr (wt.%)	/	/	0.14	0.20

The EDS elemental mapping of the Co-Cr-TiO_2 catalyst confirms the successful incorporation and spatial distribution of titanium (Ti), chromium (Cr), and cobalt (Co) within the sample. The map shows a dominant presence of Ti (represented in green), which constitutes approximately 98% of the elemental composition, indicating that the TiO_2 support is the primary matrix. Cr and Co are each detected at around 1%, visualized in orange and red, respectively.

Both dopants appear to be evenly dispersed across the TiO_2 surface, with no visible signs of clustering or localized enrichment. This homogeneous distribution suggests effective doping or surface impregnation of Cr and Co onto the support. Such uniformity is favorable for catalytic applications, as it typically leads to improved accessibility of active sites and more consistent catalytic behavior throughout the material.

These mapping results are consistent with the bulk elemental composition obtained from EDS quantification (Table 3.2), confirming the presence and successful integration of the metallic dopants.

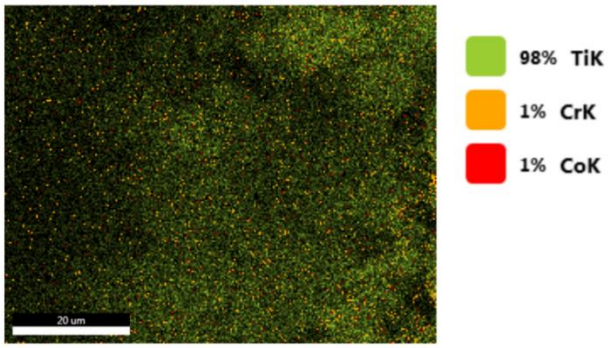

Figure 3.4. Cartography of the Co-Cr-Fe_2O_3 catalyst

Chapter 04: Experimental planning of methanol and methane production optimization

4.1. Introduction

In this work, the optimization of methanol concentration from CO_2 conversion was carried out in three main stages, using experimental design methodologies implemented with Minitab Statistical Software. The first stage focused on the development and screening of a series of heterogeneous catalysts based on Ni/TiO_2, Cr/TiO_2, and Co/TiO_2 to enhance methanol production efficiency. In the second stage, the optimization of key operational parameters influencing methanol concentration was conducted using the Box–Behnken design (BBD). The three independent variables studied in this phase were: the amount of catalyst (0.045-0.135 g), the reaction time (6-8 h), and the applied current density (20-40 mA/cm²). The third and final stage involved regenerating the catalyst and evaluating its long-term stability and reusability over successive cycles.

Additionally, a full factorial design was applied in a complementary study to investigate the electrochemical production of methane (CH_4) using the methanol as a reaction medium, which makes the electrochemical reduction of CO_2 efficient and selective for methane production [27].

4.2. Conversion of CO_2 to methanol

4.2.1. Development of a Catalyst: application of Mixture design

To enhance CO_2 dissolution and promote methanol production over the competing hydrogen evolution reaction, a composite catalyst was developed by combining three catalytic systems: Ni/TiO_2, Cr/TiO_2, and Co/TiO_2. The performance of this catalyst mixture was evaluated under controlled experimental conditions. All experiments were conducted at ambient temperature (25 °C) and atmospheric pressure (1 atm), with continuous stirring at 300 rpm. The electrochemical reaction was carried out over 6 hours, at a constant current density of 30 mA/cm². The pH of the medium was maintained in the range of 5 to 6 using a fixed H_2SO_4/Na_2SO_4 ratio of 0.2, ensuring a slightly acidic environment conducive to methanol formation.

Table 4.1. Matrix of experiments for the mixing plan case

Std	Cr-TiO_2 (g)	Ni-TiO_2 (g)	Co-TiO_2 (g)	[CH_3OH] (M)
2	0.0000	0.0450	0.0000	0.67
10	0.0075	0.0075	0.0300	0.52
8	0.0300	0.0075	0.0075	0.68
1	0.0450	0.0000	0.0000	0.70
6	0.0000	0.0225	0.0225	0.52
9	0.0075	0.0300	0.0075	0.67
3	0.0000	0.0000	0.0450	0.22
7	0.0150	0.0150	0.0150	0.60
4	0.0225	0.0225	0.0000	0.67
5	0.0225	0.0000	0.0225	0.57

To maximize methanol production yield, a statistical optimization was performed using a mixture design. By defining the lower, target, and upper bounds for each component, the optimal formulation was identified. The results indicated that the best theoretical methanol

concentration ([CH_3OH] = 0.6972M) was obtained using 0.0441 g of Cr/TiO_2 and 0.0009 g of Co/TiO_2. This solution achieved a desirability score of 1.000, reflecting perfect alignment with the optimization objectives (Figure 4.1).

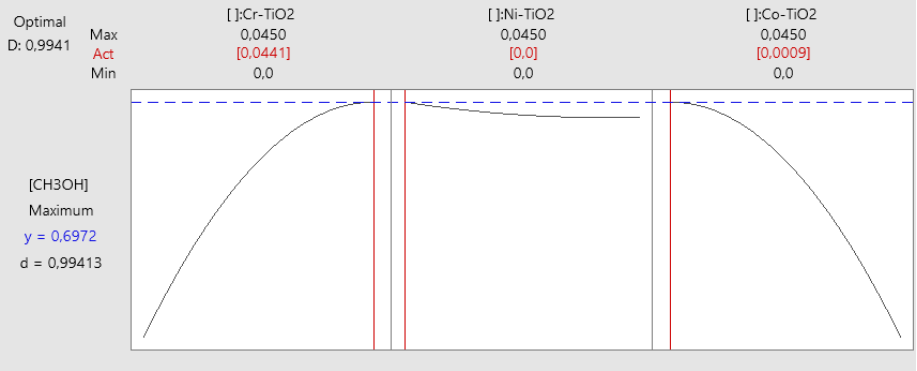

Figure 4.1. Optimization diagram.

To validate the results obtained from the optimization study, a verification experiment was conducted using the catalyst formulation corresponding to the optimal composition. Under the same operating conditions, the experimental methanol concentration achieved was 0.6667M, demonstrating good agreement with the predicted value. Encouraged by this result, a new catalyst was synthesized based on the optimized formulation and used for further parameter optimization.

4.2.2. Optimization of parameters influencing methanol production: Application of Box-Behnken design

In the second stage of this study, an additional experimental design based on the Response Surface Methodology (RSM) was carried out using the Box-Behnken Design (BBD). The aim was to maximize methanol production from CO_2 emissions using the optimized catalyst mixture developed in the previous section.

Three key process variables were selected for this investigation: reaction time (6-8 hours), current density (2-3 A/dm²), and catalyst amount (0.5-1 g). The application of the Box–Behnken Design generated an experimental matrix that systematically combined these factors at different levels, enabling the modeling and optimization of methanol yield. All experimental runs were performed according to this design, and the corresponding matrix is presented in Table 4.2.

4.2.2.1. Mathematical model

This quadratic polynomial model, generated using Minitab 21 software, expresses the relationship between methanol concentration and the studied parameters, including their interactions and squared effects, in uncoded units (eq. 4.1), and coded units (eq. 4.2).

$$[CH_3OH] = 2.94 + 21.04\, m_{catalyst} - 0.917\, t - 0.313\, I - 8.2\, m_{catalyst} \times m_{catalyst} + 0.0783\, t \times t + 0.0733\, I \times I - 2\ \times m_{catalyst} \times t - 1.111\, m_{catalyst} \times I + 0.015\, t \times I \qquad (eq\ 4.1)$$

$$[CH_3OH] = 0.6633 + 0.1\, m_{catalyst} + 0.045\, t + 0.1325\, I - 0.0167\, m_{catalyst} \times m_{catalyst} + 0.0783\, t \times t + 0.0733\, I \times I - 0.09 \times m_{catalyst} \times t - 0.05\, m_{catalyst} \times I + 0.015\, t \times I \quad (eq\ 4.2)$$

Table 4.2. Experimental matrix according to the Box-Behnken design.

Try	**$m_{catalyst}$ (g)**	**t (h)**	**I (A/dm²)**	**$[CH_3OH]_{exp}$ (M)**	**$[CH_3OH]_{theo.}$ (M)**
1	0.090	7	3	0.67	0.66
2	0.090	8	4	1.00	1.00
3	0.045	6	3	0.50	0.49
4	0.090	6	2	0.66	0.65
5	0.090	7	3	0.65	0.66
6	0.045	7	2	0.42	0.44
7	0.090	6	4	0.84	0.89
8	0.135	7	2	0.70	0.74
9	0.045	7	4	0.84	0.80
10	0.090	8	2	0.76	0.71
11	0.135	6	3	0.90	0.87
12	0.135	8	3	0.77	0.78
13	0.090	7	3	0.67	0.66
14	0.045	8	3	0.73	0.76
15	0.135	7	4	0.92	0.90

4.2.2.2. The main effects

The main effects plot provides a visual representation of the individual influence of each factor on methanol production. From the plot (figure 4.2), it is evident that the catalyst amount has a positive linear effect, as increasing its quantity leads to a higher methanol yield. In contrast, both reaction time and current intensity exhibit nonlinear effects, characterized by an initial decline in methanol production at low levels, followed by an increase at higher levels. This indicates that these two factors have a negative effect at lower values, but become beneficial beyond certain thresholds, suggesting the presence of an optimal operating range for each.

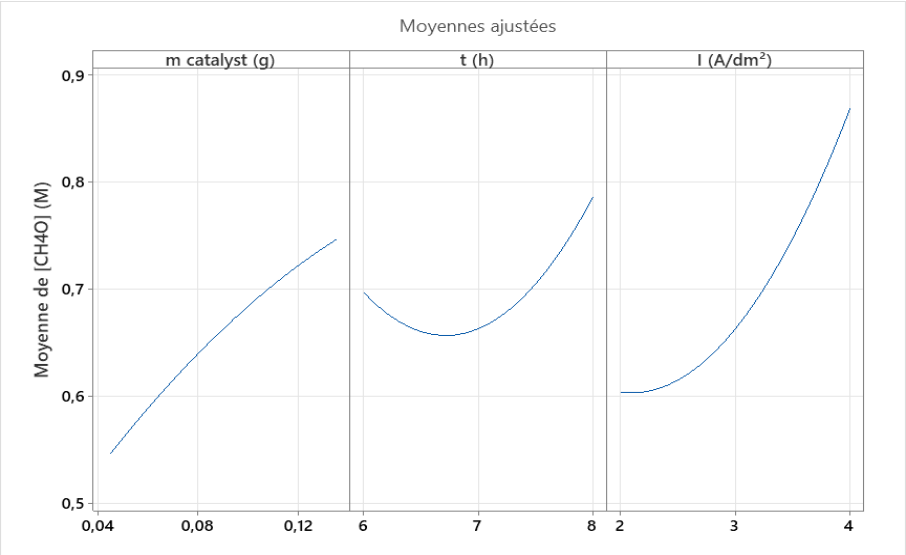

Figure 4.2. Main effects plot for methanol production.

4.2.2.3. Interaction between parameters

The interaction plots in Figure 4.3 illustrate how pairs of variables, catalyst mass ($m_{catalyst}$), reaction time (t), and current density (I), influence the methanol concentration [CH_4O], and whether these factors interact significantly.

- $m_{catalyst}$ × t: The lines diverge noticeably with increasing catalyst mass, especially at t = 6 h, showing a positive interaction, the effect of catalyst mass on methanol yield depends on the reaction time. At higher times (7-8 h), the slope becomes less steep, suggesting diminishing returns at extended durations.
- $m_{catalyst}$ × I: The three lines (I = 2, 3, 4 A/dm²) remain nearly parallel, indicating no significant interaction between catalyst mass and current density. Each factor affects methanol concentration independently within the studied range.
- t × I: This plot shows a slight curvature, particularly for I = 4 A/dm², which increases more steeply after 7 h. Although some curvature appears, the overall trend remains weak, suggesting only a mild interaction between time and current density.

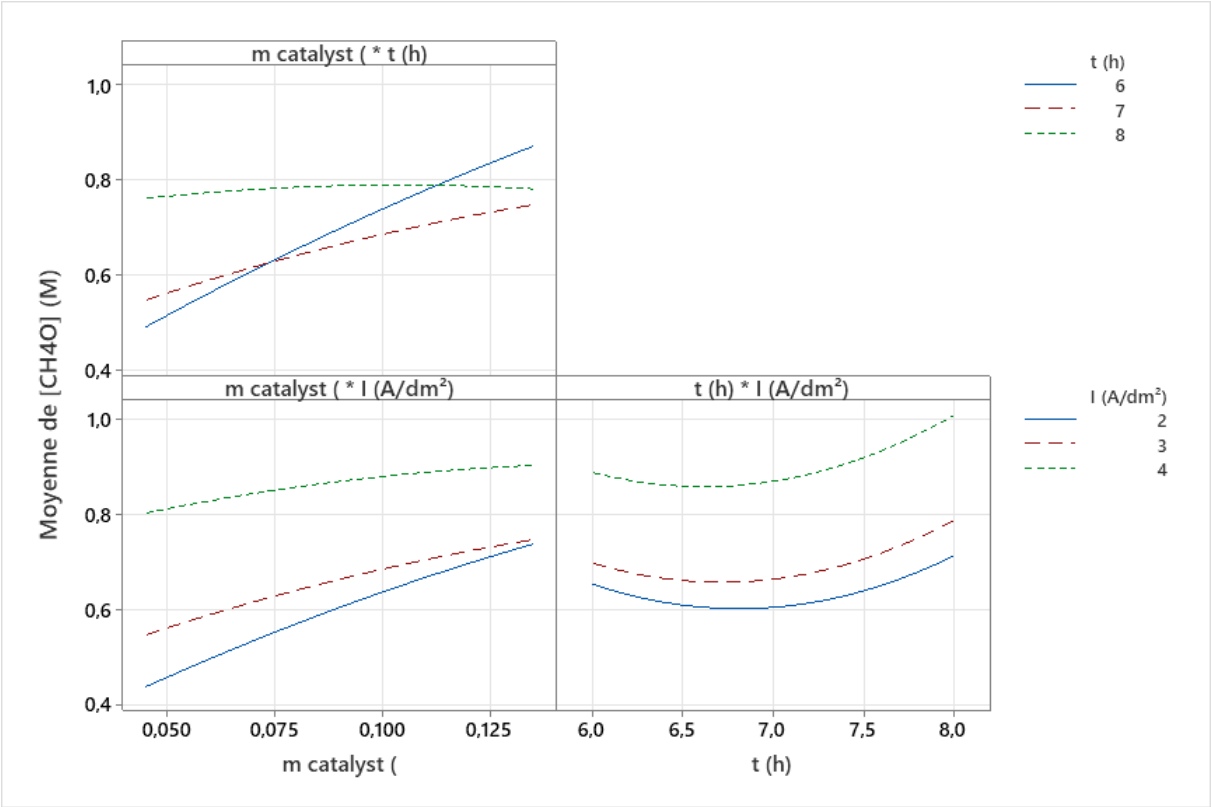

Figure 4.3. Interaction plot showing the combined effects of t, I, and $m_{catalyst}$ on methanol production.

4.2.2.4. Analysis of variance

To evaluate the statistical significance of each factor and interaction in the model, the p-values were analyzed. A p-value ≤ 0.05 indicates a statistically significant effect (with a 5% risk of error), while a p-value ≤ 0.01 suggests a highly significant effect. Effects with a p-value ≤ 0.001 are considered very strongly significant.

Based on the results presented in Table 4.3, no factors exhibit very strong significance. However, two terms show high significance: the catalyst mass (m catalyst, g) and the interaction between catalyst mass and reaction time (m catalyst × t). Additionally, three terms are statistically significant: reaction time (t), its quadratic effect (t^2), and the quadratic effect of current density (I^2).

Table 4.3. Results of the analysis of variance according to the Box-Behnken design

Source	DF	P Value
Model	9	0.003
Linear	3	0.001
m catalyst (g)	1	**0.002**
t (h)	1	**0.038**
I (A/dm²)	1	0.000
square	3	0.032

m catalyst (g)*m catalyst (g)	1	0.512
t (h)*t (h)	1	**0.021**
I (A/dm²) *I (A/dm²)	1	**0.027**
Interaction of 2 factors	3	0.031
m catalyst (g)*t (h)	1	**0.011**
m catalyst (g)*I (A/dm²)	1	0.079
t (h)*I (A/dm²)	1	0.538
Error	5	
Lack-of-fit	3	0.039
Pure error	2	
Total	14	

4.2.2.5. Contour and response surfaces

To evaluate the influence of independent variables on methanol production, both three-dimensional (3D) response surface plots and two-dimensional (2D) contour plots were generated. For clarity and conciseness, only the most relevant plots are presented in the figures below.

At the highest level of current intensity (Figure 4.3), the region corresponding to maximum methanol yield is observed when the reaction time is between 7.85 and 8 hours, and the catalyst mass is in the range of 0.01 to 0.05 g, while maintaining a constant current density of 4 A/dm³. These results suggest that increasing the reaction time has a positive effect on methanol production. In contrast, increasing the catalyst mass beyond a certain point appears to have a negative effect, as it leads to a decrease in methanol yield. This indicates that excessive catalyst loading may hinder performance, possibly due to mass transfer limitations or catalyst agglomeration.

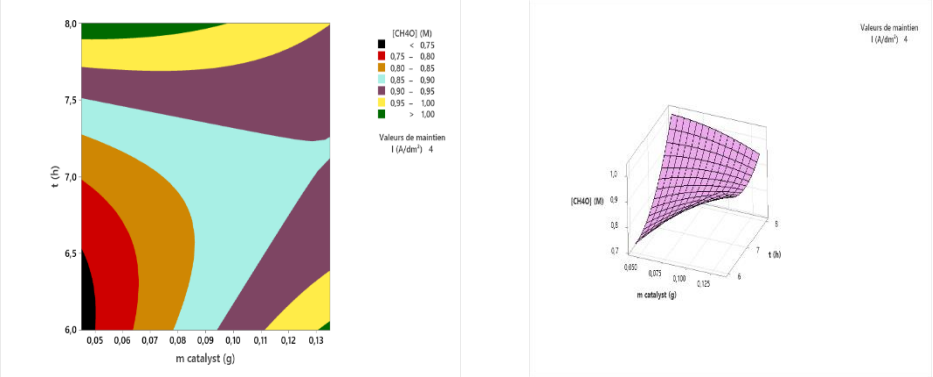

Figure 4.4. Contour and Surface Plots of $[CH_3OH]$ vs $m_{catalyst}$; t at I = 4 A/dm^2.

By setting the reaction time at 8 hours, two distinct regions can be identified in the response surface plots. The first region corresponds to low methanol concentrations ($[CH_3OH] < 0.7$ M), and is characterized by a catalyst mass below 0.08 g and a current density between 2.0 and 2.6 A/dm². The second region, where methanol concentrations exceed 1.0 M, is observed for

catalyst masses between 0.05 and 0.09 g and current densities ranging from 3.8 to 4.0 A/dm². These findings are consistent with the trends presented in the previous figure and highlight the combined influence of catalyst loading and current intensity.
Thus, it can be inferred that increasing the catalyst mass and current density promotes methanol production, up to a certain threshold beyond which the effect may stabilize or reverse depending on system limitations.

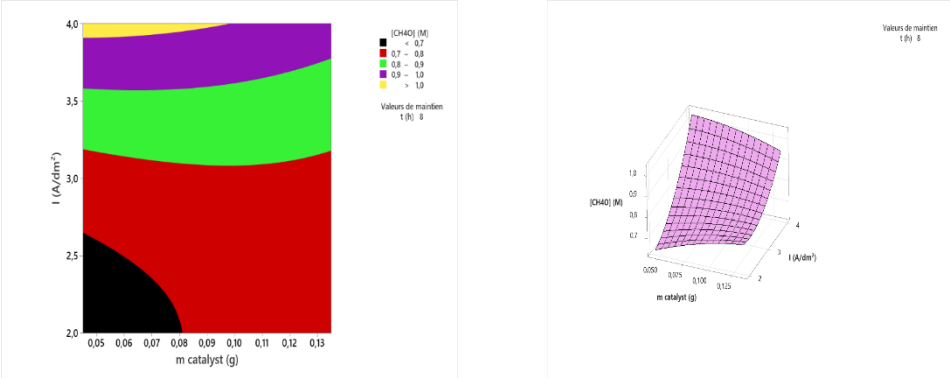

Figure 4.5. Contour and Surface Plots of [CH_3OH] vs $m_{catalyst}$; I at t = 8 hours.

At the maximum catalyst mass (m = 0.135 g), the contour plot reveals two distinct behavioral zones. A low methanol concentration region appears at longer reaction times (approximately 7 to 8 hours) and moderate current densities (around 2.5 to 3.5 A/dm²), suggesting that methanol production tends to decrease as the reaction progresses, possibly due to side reactions or degradation phenomena. Conversely, a high concentration zone is observed at shorter reaction times (around 6 hours) and higher current density (approximately 4.0 A/dm²), indicating that elevated current intensity favors rapid methanol formation in the early stages of the reaction. Overall, as reaction time increases, the concentration of methanol (CH_3OH) decreases, implying its possible transformation or consumption over time. Similarly, although higher current density initially enhances methanol production, its positive effect may be reduced during prolonged reactions. Since the catalyst mass is fixed in this representation, its influence on reaction kinetics remains constant, and the observed effects can primarily be attributed to the interaction between time and current density.

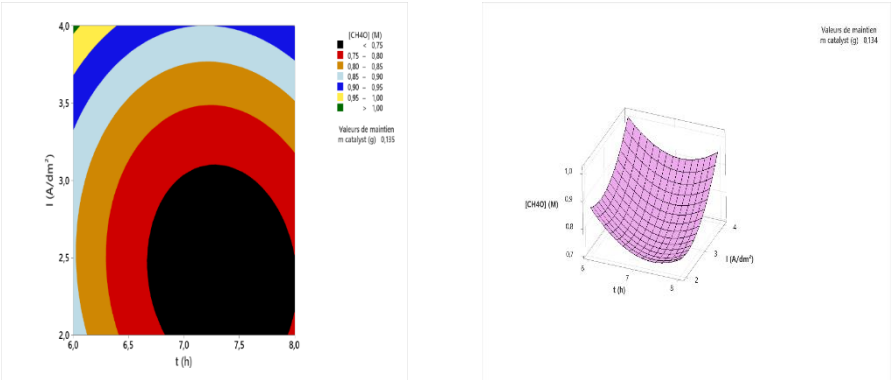

Figure 4.6. Contour and Surface Plots of [CH_3OH] vs t; I at m = 0.135 (g).

4.2.2.6. Optimization

Since the experimental design method enables the optimization of key parameters influencing methanol production, a constrained optimization was performed based on defined criteria (see optimization table). The objective was to maximize methanol concentration ([CH_3OH]) within a specified range, with a target value of 1.0 M. All factors were assigned equal weighting and importance.

Table 4.4. Optimization of the parameters.

Response	Objective	Lower	Target	Superior	weighting	Importance
[CH_3OH] (M)	Maximum	0.42	1		1	1

After multiple iterations, the best solution yielded a predicted methanol concentration of 1.0308 M, under the following optimal conditions: a catalyst mass of 0.045 g, a reaction time of 8 hours, and a current intensity of 4 A/dm². The solution achieved a composite desirability of 1.000, indicating a perfect match with the optimization criteria. The results are summarized in the optimization diagram and table below.

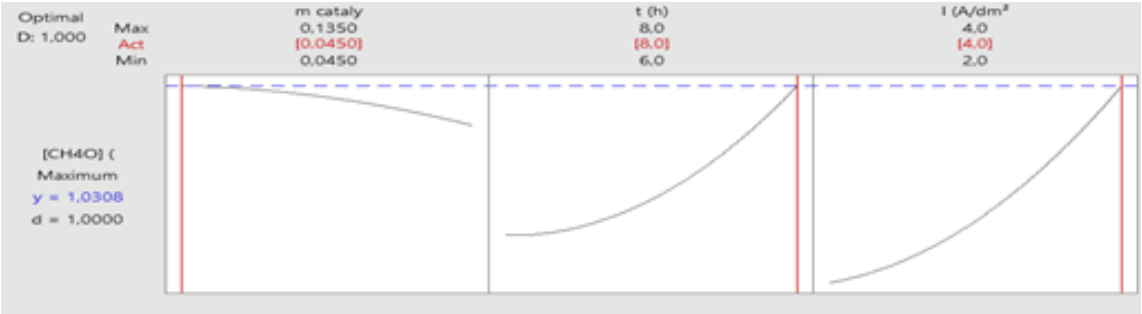

Figure 4.7. Optimization diagrams

To validate the results obtained from the optimization study, a verification experiment was conducted using the optimal conditions generated by the minitab. Under the same operating conditions, the experimental methanol concentration achieved was 0,9048M, demonstrating good agreement with the predicted value.

4.2.2.7. Catalyst Stability and Methanol Production Over Time

The catalytic stability and lifetime of the Co-Cr-TiO_2 catalyst were evaluated by monitoring methanol concentration as a function of reaction time. As shown in Figure 4.7, methanol production initially increases, reaching a maximum concentration of approximately 1.5 M after 13 hours of reaction. This peak suggests that the catalyst exhibits high initial activity and favorable kinetics for CO_2 conversion under the applied conditions: $m_{catalyst}$ = 0.0450 g, I = 4A/dm², T = 25°C, P = 1 atm, ss = 300 rpm, and pH in the range of 5 to 6.

However, beyond 13 hours, the methanol concentration begins to decrease gradually, eventually stabilizing around 0.4 M after 18 hours of reaction. This decline suggests a progressive deactivation of the catalyst, possibly due to changes in surface structure, poisoning by intermediates, or limitations in mass transfer. After this point, the catalytic activity plateaus, indicating that the system may have reached an equilibrium or that the active sites are no longer fully accessible.

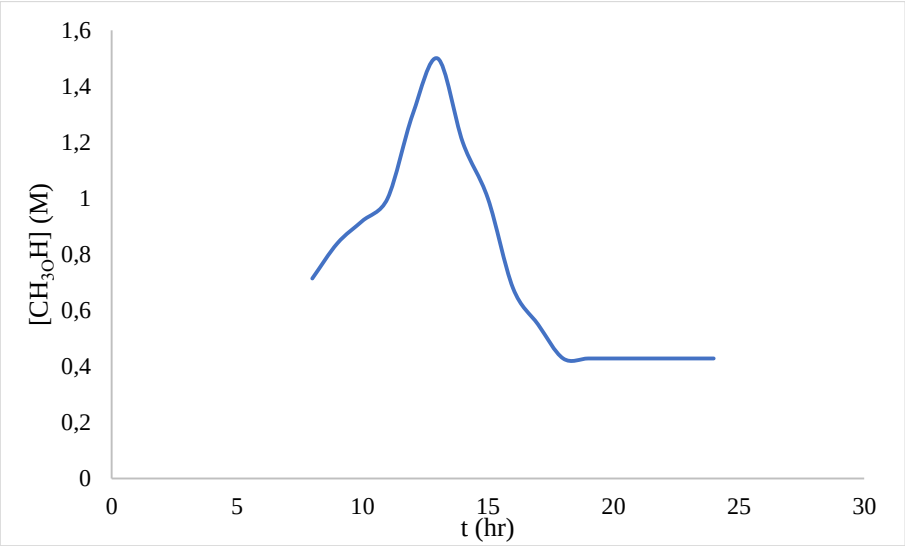

Figure 4.8. Catalyst lifetime

The deactivation of heterogeneous catalysts over time is commonly attributed to factors such as sintering of active particles**,** surface carbon deposition (coking), or formation of less active metal oxide phases. In particular, Co- and Cr-doped TiO_2 catalysts can experience reduced activity over time due to metal-support interactions or structural reorganization under reaction conditions, as supported by studies on doped TiO_2-based systems [28, 29].

These findings demonstrate that 13 hours is the optimal reaction time for maximizing methanol yield with this catalyst. Understanding this behavior is essential for determining the appropriate operational cycles and planning regeneration strategies for extended use in industrial or pilot-scale applications.

4.2.2.8. Catalyst Regeneration and Reusability Study

Following the determination of 13 hours as the optimal reaction time for maximum methanol production, the reusability of the Co-Cr-TiO_2 catalyst was evaluated through successive catalytic cycles, each lasting 13 hours. The results are shown in Figure 4.8, which presents the methanol concentration ([CH_3OH]) obtained after each cycle.

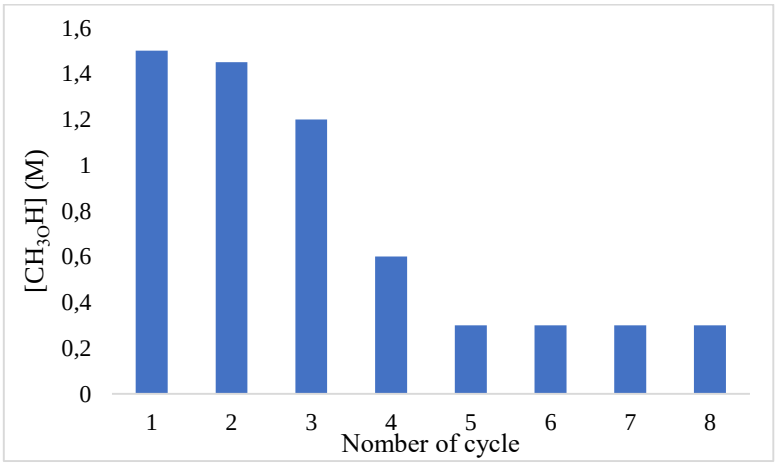

Figure 4.9. Catalyst Regeneration

During the first three cycles, the catalyst maintained relatively high activity, producing methanol concentrations of 1.48 M, 1.45 M, and 1.20 M, respectively. However, a noticeable

decline in performance was observed from the fourth cycle onward, with methanol concentrations dropping to 0.6 M in cycle 4 and below 0.3 M from cycle 5 onward. From cycles 6 to 8, the methanol concentration stabilized around 0.27 M, suggesting that the catalyst retains limited residual activity, but most of the active sites may have been deactivated.

The observed deactivation over multiple cycles may result from surface fouling, active site leaching, or structural changes in the catalyst. Similar deactivation trends have been reported for transition metal-doped TiO_2 systems under prolonged electrochemical use, often linked to loss of dopant dispersion or metal-support interactions degradation [23, 24]. These findings indicate that while the Co-Cr-TiO_2 catalyst is initially efficient, its long-term reusability is limited without proper regeneration or stabilization strategies.

4.3. Conversion of CO_2 to methane

In addition to methanol production, another promising route for CO_2 valorization is its conversion to methane (CH_4) via an electrochemical reduction pathway. In this study, we aimed to investigate the effects of temperature and applied voltage on the volume of methane produced under fixed reaction time.

To systematically evaluate the influence of these two variables, a 2^2 full factorial experimental design was employed. This approach enables the investigation of both individual effects (main factors) and interaction effects between temperature (T) and voltage (V). The design matrix ensures that all possible combinations of factor levels are tested, allowing for a comprehensive exploration of the parameter space with a limited number of experiments.

Despite its simplicity, the 2^2 factorial design provides robust insights into the system behavior and helps identify the most influential parameters affecting methane production. The matrix used for this study is shown in Table 4.5.

Table 4.5. Factorial design matrix used to study the effects of T and V on CO_2 to CH_4 conversion

Run	T (°C)	V (V)	$CH_{4exp.}$ (mL)	$CH_{4theo.}$ (mL)
1	0	1	212	212
2	21	1	23	23
3	0	3	327	327
4	21	3	45	45

4.3.1. Mathematical model

A regression equation was established to describe the relationship between the response variable, volume of methane produced (mL), and the model terms, namely temperature (T) and voltage (V). This equation provides an algebraic representation of the fitted regression model derived from the 2^2 factorial design, capturing both the main effects and the interaction between the two factors.

For this study, the resulting mathematical model is given by:

$$V_{CH_4} = 154.5 - 6.786\,T + 57.5\,V - 2.214\,T \times V \qquad (eq4.3)$$

4.3.2. Main Effects and Interaction Analysis

The influence of the studied parameters, temperature and voltage, on methane production was evaluated using main effects and interaction plots. The main effects plot (Figure 4.9) provides

insight into whether increasing the value of a given parameter results in a positive or negative impact on the response variable, i.e., the volume of CH_4 produced.

An increase in temperature from 0°C to 21°C resulted in a significant decrease in methane volume, from approximately 265 mL to 35 mL. This indicates that temperature has a negative effect on methane production under the tested conditions. In contrast, increasing the voltage from 1 V to 3 V led to a marked increase in methane yield, reaching approximately 190 mL, demonstrating a positive effect of voltage on the process.

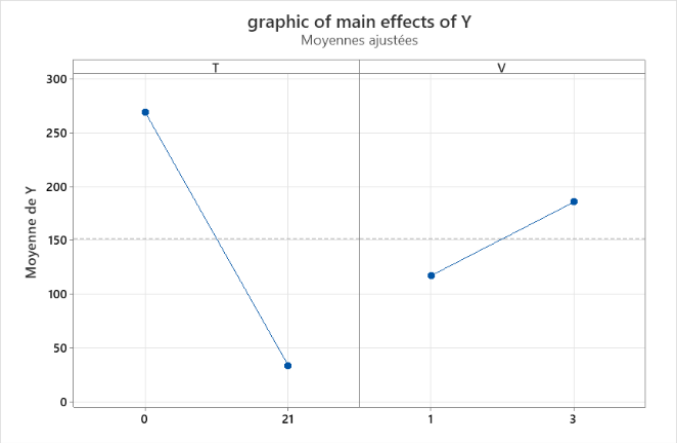

Figure 4.10. Main effects plot for methane production.

The interaction plot (Figure 4.10) explores whether the effect of one factor depends on the level of the other. Two interaction terms are considered**:** Temperature × Voltage (T×V) and Voltage × Temperature (V×T).

In the T×V interaction, at 0°C, the lines representing different voltage levels are relatively far apart, indicating distinct responses. As the temperature increases to 21°C, the lines converge, suggesting a reduction in interaction. However, the convergence remains limited, and the lines do not cross, which weakens the evidence for a strong interaction.

In the V×T plot, the lines remain nearly parallel across the voltage range (1V to 3V), reinforcing the conclusion that there is no significant interaction between the two factors.

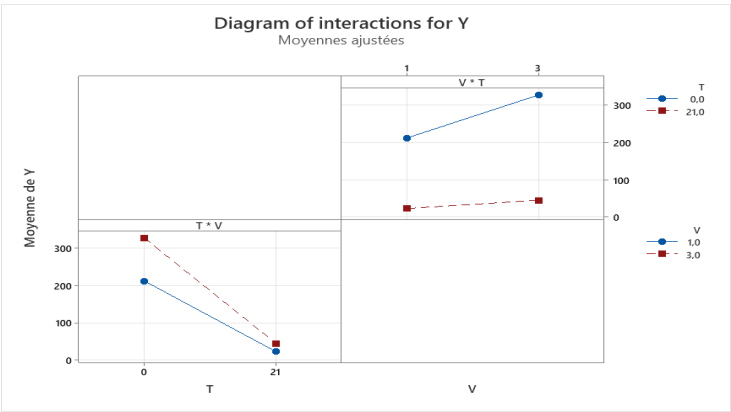

Figure 4.11. Interaction plot showing the combined effects of t and V on methane production.

4.3.3. Optimization of Methane Production

An optimization study was conducted using Minitab statistical software to identify the best combination of operating parameters (temperature and voltage) to maximize methane

production. The optimization goal was set to reach a methane volume of 350 mL, with constraints applied to the experimental domain.

Table 4.6. Optimization of input and output values

Response	Goal	Lower	Target	Higher	Weighting	Importance
Y	Maximum	23	350		1	1

According to the model, the optimal conditions were found to be at a temperature of 0°C and a voltage of 3 V, yielding a predicted response of 327 mL. Although this value does not fully meet the target, it exhibits a high composite desirability score of 0.93, indicating that the result is statistically and practically acceptable within the boundaries of the system.

This outcome confirms the earlier observations regarding factor effects: lower temperatures favor methane production, and higher voltage levels significantly enhance the conversion efficiency. As such, the recommended operational strategy involves minimizing temperature while maximizing the applied voltage, thereby validating the model's predictive capacity and the robustness of the identified optimum.

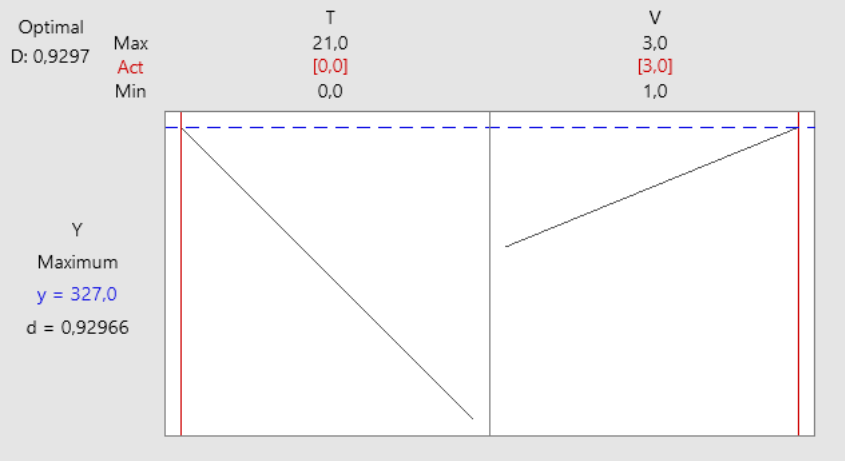

Figure 4.12. Optimization diagram

4.4. Process simulation

To evaluate the feasibility of scaling up the CO_2 conversion processes for industrial application, a simulation was performed using Aspen HYSYS V11. The complete system integrates two major processes: methanol production and methane production, both modeled using the Peng-Robinson thermodynamic package, which is well-suited for hydrocarbon systems.

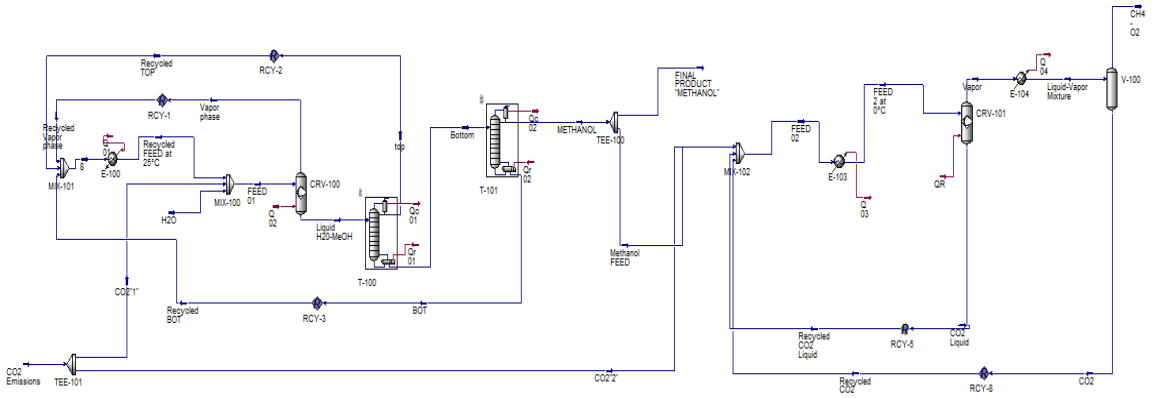

Figure 4.13. Process simulation diagram by HYSYS V11.

4.4.1. Methanol Production

The methanol production process consists of three main stages: mixing, conversion, and purification. The overall chemical reaction governing this process is:

$$CO_2 + 2\,H_2O \rightarrow CH_3OH + 1.5\,O_2$$

Initially, streams of carbon dioxide (CO_2) and water (H_2O) are combined in a mixer unit (MIX-100) under ambient temperature and pressure. This mixture is fed into an electrochemical reactor (CRV-100) where the electrocatalytic reduction of CO_2 occurs, producing methanol and oxygen.

At the reactor outlet, two main streams are formed:

- The first stream consists of unconverted CO_2 and vapor at approximately 16.08 °C, which is recycled and reheated to ambient temperature before being reintroduced into the system. This recycling helps maintain stable operating conditions.
- The second stream is a binary liquid mixture of methanol and water, which is sent to two sequential distillation columns (T-100 and T-101), each equipped with ten trays. These columns achieve methanol purification up to 80.55% at the second column's outlet.

The purified stream is split using a TEE junction (TEE-100). One portion is directed for immediate industrial use, while the other is redirected as feedstock for the methane production section.

4.4.2. Methane Production

The methane synthesis process also involves three key stages: mixing, conversion, and purification.

Due to the high solubility of CO_2 in methanol, a secondary CO_2 stream (CO_2"2") is mixed with the methanol feedstock obtained from the previous step in a mixer (MIX-102). The resulting mixture is sent to a heat exchanger (E-102) to reduce its temperature to 0 °C, which is a critical condition for the electrochemical methane production reaction.

This chilled feed is then introduced into a second electrolyzer (CRV-101), where methane is generated. The reactor output produces two flows:

- A liquid stream composed of unconverted CO_2 (aq) and methanol, which is recycled back to the mixer.
- A gas stream consisting of CO_2, O_2, CH_4, and traces of methanol.

To isolate methane and oxygen, the gaseous mixture is cooled to -150 °C to condense and separate the non-gaseous components. The remaining gaseous phase is processed via flash distillation, yielding a CH_4/O_2 mass ratio of approximately 46/53, suitable for downstream use. In real-world applications, CO_2 is typically removed using amine absorption, particularly with MEA (monoethanolamine). This process, however, could not be simulated within the current Aspen HYSYS setup because the simulation uses the Peng-Robinson equation of state, which is optimized for hydrocarbons. Accurate modeling of amine-based systems requires switching to property packages such as Amine Package or NRTL, which are specifically designed for CO_2 capture using aqueous amines.
Tables 4.7 and 4.8 summarize all the different components and flows

Table 4.7. Main Process Components

Material Streams										
		H2O	FEED 01	Vapor phase	Liquid H20-MeOH	Recycled Vapor phase	Recycled FEED at 25°C	top	Bottom	8
Vapour Fraction		0,0000	0,6859	1,0000	0,0000	1,0000	0,6880	0,0021	0,0000	0,7114
Temperature	C	25,00	25,01	21,11	21,11	21,04	25,00	-127,5	98,05	36,91
Pressure	kPa	101,3	101,3	101,3	101,3	101,3	101,3	101,3	101,3	101,3
Molar Flow	kgmole/h	80,00	2,642e+004	1,801e+004	8406	1,799e+004	2,634e+004	20,00	8386	2,634e+004
Mass Flow	kg/h	1441	7,151e+005	5,547e+005	1,604e+005	5,544e+005	7,136e+005	505,4	1,599e+005	7,136e+005
Liquid Volume Flow	m3/h	1,444	739,3	573,5	165,9	573,2	737,8	0,5882	165,3	737,8
Heat Flow	kJ/h	-2,290e+007	-3,026e+009	-6,400e+008	-2,386e+009	-6,439e+008	-3,002e+009	-5,652e+006	-2,327e+009	-2,960e+009
		Recycled TOP	BOT	Recycled BOT	METHANOL	FINAL PRODUCT "METHANOL"	Methanol FEED	CO2 Emissions	CO2"1"	CO2"2"
Vapour Fraction		0,0021	0,0000	0,0000	0,0000	0,0000	0,0000	1,0000	1,0000	1,0000
Temperature	C	-127,6	98,09	98,07	74,43	74,43	74,43	25,00	25,00	25,00
Pressure	kPa	101,3	101,3	101,3	101,3	101,3	101,3	101,3	101,3	101,3
Molar Flow	kgmole/h	20,00	8366	8327	20,00	10,00	10,00	2,727	1,363	1,363
Mass Flow	kg/h	505,3	1,593e+005	1,587e+005	556,6	278,3	278,3	120,0	60,00	60,00
Liquid Volume Flow	m3/h	0,5881	164,6	164,0	0,6719	0,3359	0,3359	0,1454	7,270e-002	7,270e-002
Heat Flow	kJ/h	-5,652e+006	-2,322e+009	-2,311e+009	-5,021e+006	-2,510e+006	-2,510e+006	-1,074e+006	-5,369e+005	-5,369e+005
		FEED 02	FEED 2 at 0°C	Vapor	CO2 Liquid	Liquid-Vapor Mixture	CH4 - O2	CO2	Recycled CO2 Liquid	Recycled CO2
Vapour Fraction		0,0002	1,0000	1,0000	0,0000	0,0016	1,0000	0,0000	1,0000	0,0000
Temperature	C	-149,7	0,0000	-5,646	-5,646	-150,0	-150,0	-150,0	-5,646	-150,0
Pressure	kPa	101,3	101,3	101,3	101,3	101,3	101,3	101,3	101,3	101,3
Molar Flow	kgmole/h	9748	9748	9752	0,0000	9752	16,00	9736	0,0000	9737
Mass Flow	kg/h	4,261e+005	4,261e+005	4,261e+005	0,0000	4,261e+005	350,6	4,258e+005	0,0000	4,258e+005
Liquid Volume Flow	m3/h	519,1	519,1	519,3	0,0000	519,3	0,7095	518,6	0,0000	518,7
Heat Flow	kJ/h	-4,051e+009	-3,810e+009	-3,810e+009	-0,0000	-4,049e+009	-8,640e+005	-4,048e+009	-0,0000	-4,048e+009

Table 4.8. Material Streams and Flow Conditions

Compositions									
	H2O	FEED 01	Vapor phase	Liquid H20-MeOH	Recycled Vapor phase	Recycled FEED at 25°C	top	Bottom	8
Comp Mole Frac (CO2)	0,0000	0,0387	0,0560	0,0000	0,0567	0,0387	0,0174	0,0000	0,0387
Comp Mole Frac (H2O)	1,0000	0,3102	0,0222	0,9242	0,0221	0,3081	0,4977	0,9252	0,3081
Comp Mole Frac (Methanol)	0,0000	0,0260	0,0032	0,0758	0,0034	0,0261	0,4829	0,0748	0,0261
Comp Mole Frac (Oxygen)	0,0000	0,5586	0,8207	0,0000	0,8203	0,5603	0,0021	0,0000	0,5603
Comp Mole Frac (Methane)	0,0000	0,0665	0,0979	0,0000	0,0976	0,0667	0,0000	0,0000	0,0667
Comp Mole Frac (TEGlycol)	0,0000	0,0000	0,0000	0,0000	0,0000	0,0000	0,0000	0,0000	0,0000
	Recycled TOP	BOT	Recycled BOT	METHANOL	FINAL PRODUCT "METHANOL"	Methanol FEED	CO2 Emissions	CO2"1"	CO2"2"
Comp Mole Frac (CO2)	0,0174	0,0000	0,0000	0,0000	0,0000	0,0000	1,0000	1,0000	1,0000
Comp Mole Frac (H2O)	0,4980	0,9267	0,9258	0,3005	0,3005	0,3005	0,0000	0,0000	0,0000
Comp Mole Frac (Methanol)	0,4826	0,0733	0,0742	0,6995	0,6995	0,6995	0,0000	0,0000	0,0000
Comp Mole Frac (Oxygen)	0,0021	0,0000	0,0000	0,0000	0,0000	0,0000	0,0000	0,0000	0,0000
Comp Mole Frac (Methane)	0,0000	0,0000	0,0000	0,0000	0,0000	0,0000	0,0000	0,0000	0,0000
Comp Mole Frac (TEGlycol)	0,0000	0,0000	0,0000	0,0000	0,0000	0,0000	0,0000	0,0000	0,0000
	FEED 02	FEED 2 at 0°C	Vapor	CO2 Liquid	Liquid-Vapor Mixture	CH4 - O2	CO2	Recycled CO2 Liquid	Recycled CO2
Comp Mole Frac (CO2)	0,9878	0,9878	0,9872	0,9985	0,9872	0,0022	0,9889	0,9985	0,9888
Comp Mole Frac (H2O)	0,0003	0,0003	0,0000	0,0000	0,0000	0,0000	0,0000	0,0000	0,0000
Comp Mole Frac (Methanol)	0,0007	0,0007	0,0000	0,0000	0,0000	0,0000	0,0000	0,0000	0,0000
Comp Mole Frac (Oxygen)	0,0022	0,0022	0,0029	0,0002	0,0029	0,3636	0,0023	0,0002	0,0022
Comp Mole Frac (Methane)	0,0090	0,0090	0,0099	0,0013	0,0099	0,6343	0,0089	0,0013	0,0090
Comp Mole Frac (TEGlycol)	0,0000	0,0000	0,0000	0,0000	0,0000	0,0000	0,0000	0,0000	0,0000

General Conclusion

This study aimed to convert carbon dioxide (CO_2) emissions into valuable hydrocarbons, specifically methanol and methane, via two distinct processes: the electrocatalytic reduction of CO_2 to methanol and the electrochemical reduction of CO_2 to methane.

The first axis focused on methanol production and encompassed catalyst development, optimization of reaction parameters, and evaluation of catalyst durability. Among the synthesized materials, the Co-Cr/TiO_2 catalyst exhibited the most promising performance, achieving up to 1.0308 M of methanol under optimal conditions (0.045 g catalyst, 8 h, 4 A/dm²). Extended operation showed a peak yield of ~1.5 M after 13 hours, followed by a gradual decline to ~0.4 M, indicative of catalyst deactivation. Regeneration tests across eight cycles revealed substantial activity loss beyond the third cycle, with methanol concentration stabilizing around 0.27 M.

The second axis investigated CO_2-to-methane conversion, leveraging the high solubility of CO_2 in methanol. Optimal conversion was obtained at 0 °C and 3 V, producing 327 mL of CH_4/O_2, suggesting potential use as an industrial fuel.

To assess scalability, a process simulation using Aspen HYSYS V11 was carried out, demonstrating the feasibility of integrating both conversion routes through mixing, reaction, and purification units.

Overall, this study confirms that CO_2 can be efficiently converted into energy-dense products using low-temperature, electrocatalytic technologies. Future research could aim at improving catalyst stability, exploring alternative dopants, and scaling up electrolyzer designs. Such processes, powered by renewable energy, align with sustainable development goals and offer a viable path for mitigating greenhouse gas emissions.

References

1. International Monetary Fund. (2024, March 7). *Algeria: Selected issues – Fiscal reforms to support addressing climate change challenges* (IMF Country Report No. 24/89).
2. Climate Analytics. (2023). *Algeria – Pathways to 1.5°C compatible emissions reductions*. https://1p5ndc-pathways.climateanalytics.org/countries/algeria.com
3. Green Steel World. (2022). *Tosyali Algeria: Pioneering green steel in North Africa*. https://greensteelworld.com
4. Prozesswärme. (2022). *Tosyali Algeria sets DRI production record in 2021*. https://prozesswaerme.net
5. Zhang, Y. et al. (2022). *Catalytic CO_2 Hydrogenation to Methanol: From Mechanism to Industrial Practice*. ChemCatChem, 14(5), 1-15.
6. Li, X. et al. (2023). *Designing stable Cu-based catalysts for efficient CO_2 hydrogenation to methanol*. Applied Catalysis B, 328, 122515.
7. Xu, R. et al. (2021). *Water effect on methanol synthesis from CO_2 over Cu/ZnO catalysts*. Journal of CO_2 Utilization, 46, 101481.
8. Chen, M. et al. (2023). *Promoter effects in CO_2 hydrogenation: The role of ceria and gallium*. ACS Catalysis, 13(2), 1082–1095.
9. Nguyen, T. et al. (2024). *Ni-based catalysts for CO_2 methanation: Advances and challenges*. Renewable and Sustainable Energy Reviews, 185, 113520.
10. Wang, J. et al. (2022). *CO_2 hydrogenation over Ru-based catalysts: Kinetics and stability*. Energy & Fuels, 36(10), 5076–5085.
11. Kumar, A. et al. (2025). *Nanostructured catalysts for efficient CO_2 valorization: A pathway toward circular carbon economy*. Nature Catalysis, 8(1), 40–55.
12. Torres, L. et al. (2023). *Challenges in scaling CO_2 hydrogenation: From lab to industry*. Chemical Engineering Journal, 458, 141293.
13. Lucile, F., Cézac, P., Contamine, F., Serin, J.-P., Houssin, D., & Arpentinier, P. (2012). Solubility of carbon dioxide in water and aqueous solution containing sodium hydroxide at temperatures from (293.15 to 393.15) K and pressure up to 5 MPa: Experimental measurements. *Journal of Chemical & Engineering Data, 57*(3), 784–789.
14. Chen, Q., et al. (2023). *Pressure and temperature effects on CO_2 solubility in electrochemical systems*. Journal of Electroanalytical Chemistry, 931, 117262.
15. Zhang, Y., & Wang, G. (2022). *Copper as an efficient catalyst for CO_2 reduction to multi-carbon products*. Nature Catalysis, 5(3), 234–245.
16. Kim, D. et al. (2023). *Mechanistic insights into CO_2 reduction on Cu electrodes*. ACS Energy Letters, 8(2), 642–651.
17. Lee, J., et al. (2021). *Influence of pH on CO_2 speciation and electroreduction efficiency*. Electrochimica Acta, 388, 138630.
18. Sun, X., et al. (2024). *Competition between CO_2RR and HER in acidic media*. Advanced Functional Materials, 34(1), 2307812.
19. Wang, H., et al. (2023). Rational catalyst design for selective electrochemical CO_2 reduction. Chemical Society Reviews, 52(4), 2032–2055.
20. Ren, Y., et al. (2025). *Suppressing hydrogen evolution in electrocatalytic CO_2 reduction: A catalyst perspective*. Energy & Environmental Science, 18(2), 413–428.

21. Liu, K., et al. (2022). *Gas-diffusion electrodes for high-performance CO_2 electroreduction***.** Nature Reviews Materials, 7(9), 735–749.
22. Torres, L., et al. (2023). *Advances in nanostructured catalysts for CO_2 electroreduction*. Journal of Catalysis, 417, 12–28.
23. Zhang, Y., et al. (2023). *Homogeneous nickel and cobalt complexes for low-overpotential CO_2 reduction*. ACS Catalysis, 13(4), 2210–2222.
24. Chen, M., et al. (2022). *Polymeric metal-metal catalysts for selective electrochemical formic acid production*. Journal of Materials Chemistry A, 10(12), 5470–5481.
25. Li, X., et al. (2024). *Molybdenum carbide nanoparticles on N-CNTs for efficient methanol electrosynthesis from CO_2*. Advanced Functional Materials, 34(2), 2309871.
26. Nguyen, T., et al. (2025). *Pyridine-derived organohydride catalysts for selective CO_2-to-methanol electroreduction*. Nature Communications, 16(1), 1023.
27. Kaneco, S., et al. (2006*). Electrochemical reduction of CO_2 to methane at the Cu electrode in methanol with sodium supporting salts and its comparison with other alkaline salts*. *Energy & Fuels*, 20(1), 409–414.
28. S. Zhao, et al., "Influence of transition metal doping on the stability and activity of TiO_2-based catalysts for CO_2 conversion," *Applied Surface Science*, vol. 489, pp. 102–109, 2019.
29. Y. Liu, et al., "Deactivation mechanisms of Co- and Cr-based oxide catalysts in methanol synthesis from CO_2," *Journal of Catalysis*, vol. 374, pp. 58–68, 2019.